Received May 16, 2018, accepted June 12, 2018, date of publication June 25, 2018, date of current version July 19, 2018.

Digital Object Identifier 10.1109/ACCESS.2018.2849929

Modelling of a 400-kV MSCDN Reactor for Computation of Voltage and Field Distributions During Switching Transients

HAZIAH ABDUL HAMID[1], (Member, IEEE), NOUREDDINE HARID[2], (Member, IEEE), MANU A. HADDAD[3], (Member, IEEE), AND HUW GRIFFITHS[2], (Member, IEEE)

[1]School of Electrical Systems Engineering, Universiti Malaysia Perlis, Pauh Putra Campus, Arau 02600, Malaysia
[2]Department of Electrical and Computer Engineering, Khalifa University of Science and Technology, Abu Dhabi 2533, United Arab Emirates
[3]School of Engineering, Cardiff University, Cardiff CF24 3AA, U.K.

Corresponding author: Noureddine Harid (noureddine.harid@ku.ac.ae)

ABSTRACT In this paper, a model for the reactor of a 400-kV mechanically switched capacitor with damping network (MSCDN) based on an equivalent circuit representation is developed. The model is based on sub-dividing the physical reactor into sections which are sufficiently small to be represented by a lumped-parameter equivalent circuit. The circuit parameters are obtained for each section using analytical formulae based on the physical configuration of the reactor, the winding layout, and the insulation material. The model is then simulated in the ATP/EMTP program for the evaluation of transient voltage and field distributions along of the reactor. This helps in identifying possible failure scenarios which will allow designing measures to mitigate failures effectively during transients arising from switching operations. Further analysis of the results has revealed that there are substantial dielectric stresses imposed on the winding insulation that can be attributed to a combination of three factors. First, the surge arrester operation during the MSCDN energization, which causes steep voltage change at the reactor terminal. Second, the non-uniform voltage distribution, resulting in high stresses across the top inter-turn windings. Third, the rapid rate-of-change of voltage in the assumed worst-case reactor winding location. This is accompanied by a high dielectric (displacement) current through the inter-turn winding insulation. The results of this paper indicate that a synergistic effect of high electric field and high dielectric current occurring at worst energization, followed by the thermal effects of steady state operation may contribute to the failure of air-core reactors used on the 400-kV MSCDN.

INDEX TERMS Reactor, mechanically-switched capacitor, equivalent circuit, transient overvoltage, ATP/EMTP.

I. INTRODUCTION

Mechanically-switched capacitors with damping network (MSCDN) offer various benefits for electrical power transmission systems, such as voltage control, reactive power control, improvement of system stability, prevention of voltage instability, and reduction of system harmonics. During service, the MSCDN is subject to frequent switching operations and system perturbations, which may expose its components to transient overvoltages and currents with high rate of rise and long duration [1]. Of these components, the filter reactor, which is of dry type air-core design, may be particularly vulnerable to multiple overvoltage stresses produced during energisation [2]. With steep wave front impulse voltages, the voltage distribution on the reactor is non-uniform. Studies have shown that turn-to-turn insulation failure at the HV end of the reactor is the most common problem encountered during their service operation [3]. Such a failure may cause short circuit of turn-to-turn insulation, which consequently damages the reactor due to excessive overvoltages. This problem may occur if the applied electric field exceeds the dielectric strength of the insulation [4], [5]. Factors that influence the dielectric strength include the magnitude, shape, duration and polarity of the applied voltage, the operating temperature, and other physical states of the insulation [6]. For solid dielectric materials, destructive stresses in electrical insulation systems are usually caused by one or any combination of electrical, mechanical, thermal, and environmental factors.

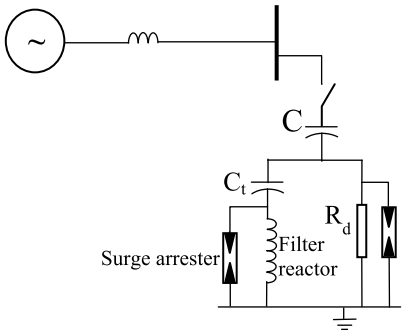

FIGURE 1. Simplified topology of MSCDN and filter reactor. C: main capacitor, C_t: tuning capacitor, R_d: damping resistor.

Work on the analysis of voltage distribution on reactor windings is available in the literature [7]–[13]. Referring to the simplified equivalent circuit shown in Fig. 1, the reactor of the MSCDN and filter reactor consist of an inductance and a capacitance tuned to the system frequency for minimising steady state losses, and a tuning capacitance in series with the reactor to minimize harmonic amplification during transients. A damping resistor is used for damping the harmonic voltages. Both reactor and damping resistor are protected against overvoltages by surge arresters. Such a model can only provide information about the overvoltages generated at the reactor terminals. A more accurate model should contain sufficient detail to represent the physical reactor and reproduce the reactor's behaviour during switching transients. This requires inclusion of each turn with all inductive and capacitive mutual couplings. Different approaches have been used to model windings for the computation of transient voltage distribution.

Lumped-parameter circuit representation is one of the approaches that satisfy such requirements, and was used by [11] and [14] to model the transient response of windings. Another approach, based on transmission line modelling, and which considers the frequency-dependent core and copper losses, was proposed to compute very fast transients on transformer windings [10]. Enohnyaket [15] presented a model of air-core reactors based on partial element equivalent circuit (PEEC) which can be used in both time and frequency domain analysis, but this is computationally excessive.

This paper proposes a detailed model representing a single-layer air-core reactor based on the lumped-parameter approach, with the stray components included. The parameters are derived based on the physical geometry, the winding configuration and the insulation material of the reactor. The model is implemented in the ATP/EMTP program to compute the distribution of voltage and then calculates the electric field along the reactor winding. Equations for the electric field stresses on the winding insulation, including the derivation of a relationship between the maximum generated overvoltage and the main winding parameters, are derived. The model also computes the inductive and capacitive currents in each section of the reactor winding. A parametric analysis of the failure mechanisms in the reactor parts is carried out to determine the most influential factors on the dielectric strength.

II. DERIVATION OF LUMPED PARAMETER EQUIVALENT CIRCUIT

The winding is divided into short sections in which the conductive current is approximately constant [16]. This subdivision allows the winding section to be represented by a lumped-parameter equivalent circuit. Fig. 2(a) shows a physical reactor and Fig. 2(b) illustrates the division of the winding into k equal, short-length sections and their location above ground. For the numerical application, the air-core reactor investigated in this study has a height of 2.65 m and an inner diameter of 0.9 m. The winding conductor is made of aluminium and has a diameter of 2 mm, and is insulated by Mylar polyester film of 50 μm thickness. A lumped parameter approach can then be used to analyse the reactor's transient response, as shown in Fig. 2(c). The parameters of the equivalent circuit are derived as described in the following sections.

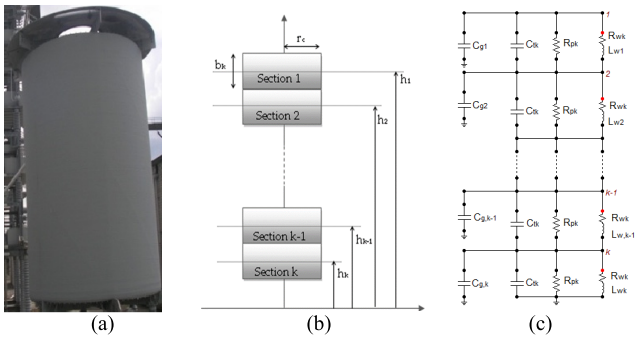

FIGURE 2. Modelling of aire-core winding (a) Physical reactor (b) winding subdivision (c) equivalent circuit, h_k: height above ground of the centre of section k, r_c: radius of the reactor, b_k: length of section k.

A. SELF AND MUTUAL INDUCTANCES

The self-inductances of the winding conductors were computed using the following formula [17]:

$$L_{sw} = \frac{0.002\pi^2 a_t^2 N_k^2 K}{b_k/2a_t} \quad (1)$$

where: L_{sw}: self-inductance of section k (mH), a_t: mean section radius (cm), N_k: number of turns of section k, b_k: length of section k (cm). The constant K ($0 \leq K \leq 1$) is tabulated as a function of the coil diameter and length.

The mutual inductances between two coils were obtained based on the coaxial geometry shown in Fig. 3, where $2m_1$ is the axial length of Coil 1 and a_t its radius, $2m_2$ is the axial length of Coil 2 and A_t its radius. The separation between the coil centres, s indicates whether, the coils are partially inside, completely inside, or completely outside each other.

The mutual inductance between reactor sections is:

$$M_{k,k+1} = 0.002\pi^2 a_t^2 n_k^2 [r_1 B_1 - r_2 B_2 - r_3 B_3 + r_4 B_4] \quad (2)$$

TABLE 1. Self and mutual inductances of winding sections (mH).

k	1	2	3	4	5	6	7	8	9	10
1	18.245	7.713	2.896	1.359	0.720	0.418	0.260	0.172	0.119	0.086
2	7.713	18.245	7.713	2.896	1.359	0.720	0.418	0.260	0.172	0.119
3	2.896	7.713	18.245	7.713	2.896	1.359	0.720	0.418	0.260	0.172
4	1.359	2.896	7.713	18.245	7.713	2.896	1.359	0.720	0.418	0.260
5	0.720	1.359	2.896	7.713	18.245	7.713	2.896	1.359	0.720	0.418
6	0.418	0.720	1.359	2.896	7.713	18.245	7.713	2.896	1.359	0.720
7	0.260	0.418	0.720	1.359	2.896	7.713	18.245	7.713	2.896	1.359
8	0.172	0.260	0.418	0.720	1.359	2.896	7.713	18.245	7.713	2.896
9	0.119	0.172	0.260	0.418	0.720	1.359	2.896	7.713	18.245	7.713
10	0.086	0.119	0.172	0.260	0.418	0.720	1.359	2.896	7.713	18.245
Total	31.901	39.528	42.305	43.492	43.952	43.952	43.492	42.305	39.616	31.989

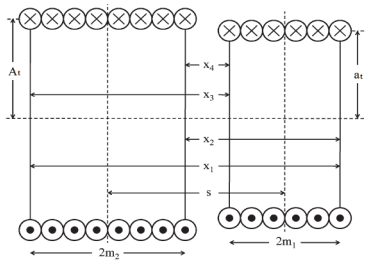

FIGURE 3. Basic geometry of two coaxial single-layer coils.

where $M_{k,k+1}$ mutual inductance between sections k and $k+1$ (mH) and a_t the mean radius (cm), n_k the winding density (turns/cm), r_n diagonal distances between sections (cm) and B the elliptic integral values.

The four elliptic integrals, are functions of the following four axial distances

$$\begin{aligned} x_1 &= s + (m_1 + m_2) \\ x_2 &= s + (m_1 - m_2) \\ x_3 &= s - (m_1 - m_2) \\ x_4 &= s - (m_1 + m_2) \end{aligned} \tag{3}$$

The diagonal distances between sections are given by

$$r_i = \sqrt{x_i^2 + A_t^2}, \quad i = 1..4 \tag{4}$$

The elliptic integral values are tabulated as a function of the following constants:

$$\rho_n^2 = \frac{A_t^2}{r_n^2} \tag{5}$$

$$\alpha = \frac{a_t}{A_t} \tag{6}$$

The total inductance L_{wk} of section k is the sum of its self-inductance and the mutual inductances due to all other sections. Table 1 summarizes the calculated self and mutual inductances for each section of the reactor winding for $k = 10$. The diagonal elements of the table are the self-inductance of each winding section. The off-diagonal elements are the mutual inductance between sections.

B. WINDING SERIES RESISTANCE

The series resistance R_{wk} represents the total winding ohmic losses, the proximity effect, and the stray field losses caused by the large transverse magnetic field to which the conductors are subjected. Under impulse condition, the dielectric or shunt losses of the reactor are more dominant than the series losses; therefore, the latter can be adequately represented by the ohmic losses of winding only. Assuming uniform current distribution across the winding cross-section and that the current remains constant at a dominant frequency, the series resistance of section k of the winding can be estimated as

$$R_{wk} = \frac{2N_k \rho_c r_c}{r_w^2} \tag{7}$$

where N_k is the number of turns in section k, ρ_c the conductor resistivity, r_c the section radius and r_w the conductor radius.

C. INSULATION THICKNESS

The thickness of insulation in one turn layer (insulation between two successive turns of the winding) is assumed to be equal to twice the thickness t_m of the conductor insulating material. For a coil having N turns of conductors, the total insulation thickness in the coil is:

$$t_h = N \times 2t_m \tag{8}$$

The height of each coil can then be obtained from:

$$h_x = N\,(2t_m + 2r_w) \tag{9}$$

from which we obtain:

$$t_h = \frac{h_x}{1 + \left(r_w/t_m\right)} \tag{10}$$

D. INTER-TURN INSULATION RESISTANCE

The current through the inter-turn insulation is composed of the capacitive current associated with field changes in the dielectric, the absorption current due to polarization effects and the conduction or leakage current due to the actual electronic conduction [18]. Leakage current represents the steady state of the dielectric current that relies upon the applied electric field and temperature. The shunt resistance R_{pk} of section k of the inter-turn winding insulation is calculated from:

$$R_{pk} = \frac{(N_k - 1)\,\rho_m t_m}{\pi^2 r_c r_w} \tag{11}$$

Where ρ_m is the resistivity of insulating material and t_m its thickness. The effective area is taken equal to half of the area of the conductor surface of the inter-turn winding.

This resistance can also be calculated at a given frequency f if the dissipation factor (tanδ) of the insulation, and the inter-turn capacitance are known:

$$R_{pk} = \frac{N_k}{2\pi f C_{tt} tan\delta} \tag{12}$$

where $tan\delta$ is the dissipation factor, f the dominant frequency, and C_{tt} the inter-turn capacitance.

E. INTER-TURN CAPACITANCE

Assuming a small thickness of the insulation coatings, it is possible to calculate the equivalent capacitance $C_{t,k}$ of the series connected inter-turn capacitances of section k by approximating the conductor surfaces with a parallel-plate having an effective area equal to half of the conductor cylindrical surface:

$$C_{tt,k} = \frac{2\pi^2 \varepsilon_0 \varepsilon_m r_c r_m / t_m}{N_k - 1} \tag{13}$$

where ε_0 is the permittivity of vacuum (F/m), and ε_m is the relative permittivity of the dielectric (F/m).

F. CAPACITANCE TO GROUND

The stray capacitances-to-ground C_{gk} of each section can be calculated for a vertical cylinder [18] as:

$$C_{gp} = \pi \varepsilon_o d_c \left[\frac{\pi d_c}{2h_k} + \ln\left(1 + \frac{b_k}{h_k}\right) \right] \tag{14}$$

where: d_c is the conductor diameter, b_k length of section k and h_k distance from the centre of section k to ground.

III. MODEL IMPLEMENTATION IN ATP/EMTP

Fig. 4 shows the complete simulation circuit with a detailed model of the reactor added to the MSCDN network. To investigate surge voltage distribution, the circuit breaker is specified to close at the instant of voltage maximum, replicating worst switching conditions. The computation time step is 10 ns and the total simulation time is 10 ms. The closing time of the switch representing the circuit breaker is specified at 2 ms, which was adjusted correspondingly to the time of maximum supply voltage. For the distribution of voltage and

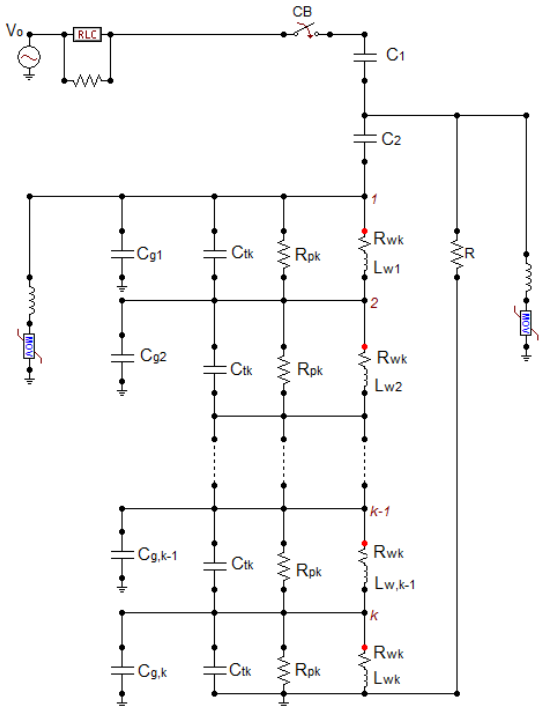

FIGURE 4. ATP/EMTP simulation circuit for the MSCDN.

electric field at each reactor section, the maximum values are considered, and the results are reported in the following sections.

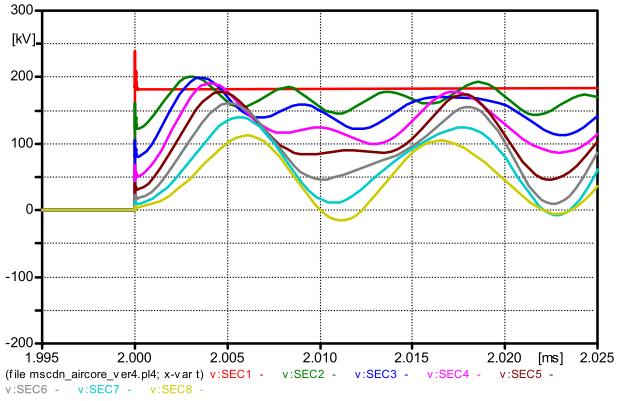

FIGURE 5. Node voltage to ground (Vsec1 to Vsec8 indicate the computed voltages at the 0%, 10%, 20% up to 70% along the winding away from the top HV terminal).

IV. VOLTAGE DISTRIBUTION ALONG MSCDN REACTOR

A. DISTRIBUTION OF NODE TO GROUND VOLTAGE

Fig. 5 shows transient voltage-to-ground waveforms generated at different locations on the reactor winding following MSCDN energization. The voltage waveform Vsec1 is the voltage-to-ground measured at the reactor terminal, which reaches the highest magnitude of approximately 225 kV at an instant t = 5ns after switch closing. The actual steady state reactor voltage is approximately 50 kV. The waveforms

Vsec2 to Vsec8 representing the node voltages occurring at 10% to 70% of the reactor winding, have complex damped oscillatory shapes of different oscillating frequencies. The voltage to ground along the winding length was also computed at time instants between 0.5 μs and 2 μs after switching, with a time interval of 0.5 μs. The voltage distribution is non-uniform, as shown in Fig. 6, because of stray capacitances to both inter-turn and ground couplings. At the start of the transient, the highest stresses were observed at the top of the winding. As the impulse propagates along the winding, the voltage is redistributed towards the middle of the coil and away from the top. This non-uniformity should be kept to a minimum to avoid damage to upper parts of the reactor winding, which are inevitably more stressed.

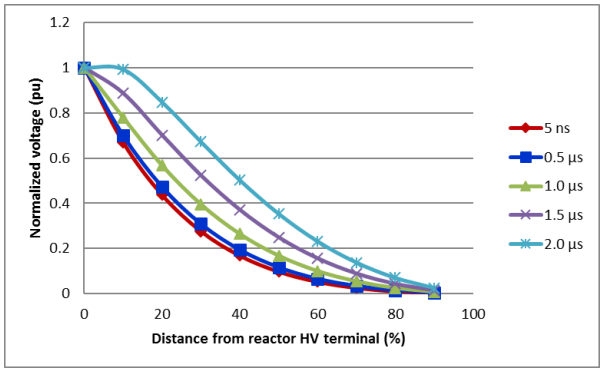

FIGURE 6. Distribution of node to ground voltages at different times following energization of the MSCDN.

In Fig. 6, the voltage values normalised to the highest voltage magnitude computed at each time instant are shown.

Considering only the results obtained at time 5 ns, which reflect the worst energising transient, it is possible to approximate the normalised voltage distribution by an exponential function. Based on this approximation, the voltage $V(x)$ at any point along the reactor can then be written as:

$$V(x) = V_m \left(1 - e^{-0.04013x}\right) \tag{15}$$

where x is the distance from the reactor terminal (%), and V_m is the maximum value of voltage occurring on the reactor.

B. DISTRIBUTION OF NODE-TO-NODE VOLTAGE

The peak values of the voltage differences appearing between winding sections following energization, i.e. Vsec1-Vsec2, Vsec2-Vsec3 . . . Vsec7-Vsec8, which correspond respectively to the voltages across sections of the model, are shown in Fig. 7. The highest magnitude is found across the first section at the top of the reactor winding, where a magnitude of approximately 80 kV is imposed. This voltage appearing across only one-tenth of the reactor produces a high stress on the turn-to-turn insulation in that part of the reactor. The stress is approximately evenly distributed between sections starting from the third section of the reactor towards the ground. Tests on a laboratory scale model would be useful for validating the model results.

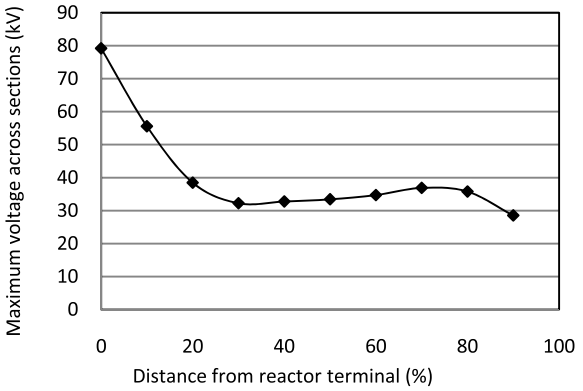

FIGURE 7. Distribution of maximum node-to-node voltages following energization of the MSCDN.

C. CAPACITIVE AND INDUCTIVE CURRENTS

Fig. 8(a) shows the current flow through the reactor winding (I_L) and the current through the winding insulation (I_C) after the energisation of the MSCDN. The current I_C is the capacitive current flow through the stray inter-turn capacitances of the reactor winding and is shown on expanded timescale in Fig. 8(b). This current is dependent on the switching instant of the closing circuit breaker and the voltage change at the reactor terminal. Its magnitude reaches more than 300 A in just a few microseconds following energisation, during which the current through the reactor winding is almost negligible. This may initiate degradation and create weak points in the insulation, which may worsen through thermal effects on application of main voltage during in-service duty.

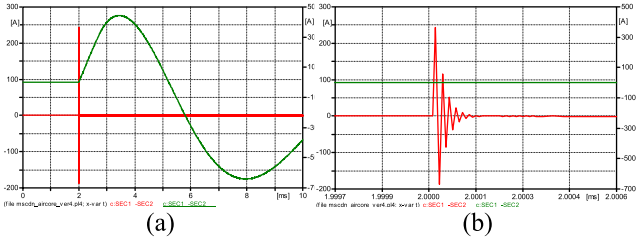

FIGURE 8. Capacitive current, I_C (left scale) through the inter-turn capacitance and current in the reactor winding I_L (right scale). (a) Inductive current (b) Capacitive current (expanded).

V. FIELD DISTRIBUTION ALONG MSCDN REACTOR

A. INTER-TURN ELECTRIC FIELD STRENGTH

The electric field intensity at points located in the top 10% of the reactor winding can be calculated by assuming it uniform throughout the dielectric in that small region, and that the potential varies linearly. This assumption is made to nullify the effect of field distortion due to fringing effect of the line forces. Combining Equations (10) and (15), the average electric field E_{av} can be written as:

$$E_{av} = \frac{V_m}{h_x}\left(1 + \frac{r_w}{t_m}\right)\left(1 - e^{-bx}\right) \tag{16}$$

where V_m is the maximum voltage and b is a constant. This equation shows that for a particular voltage distribution, the electric field strength is influenced by the physical geometry of the reactor winding and the maximum applied voltage, which in turn depends on the time at which the maximum overvoltage occurs.

TABLE 2. Values of constants b and V_m for different times.

Time	5 ns	0.5 µs	1 µs	1.5 µs	2 µs
b	0.04	0.036	0.025	0.012	0.001
V_m (kV)	229.21	182.23	182.25	182.26	182.28

To calculate the electric field strength, the constants V_m and b were first calculated from the voltage distributions analysed in the previous section, and the results are summarized in Table 2. The average field obtained for the upper 10% section of the winding length is shown in Fig. 9. This field was computed based on an insulation thickness of 100 μm, with the highest value of approximately 73 kV/cm at 5 ns following energisation. For this 5-ns instant, the field intensity along this part of the winding decreases by only 17%. The field decreases with time after energisation. At the later time instants, the field tends to become more uniformly distributed along the upper 10% length of the reactor. The results indicate that there may be implications on the winding insulation after a large number of switching operations.

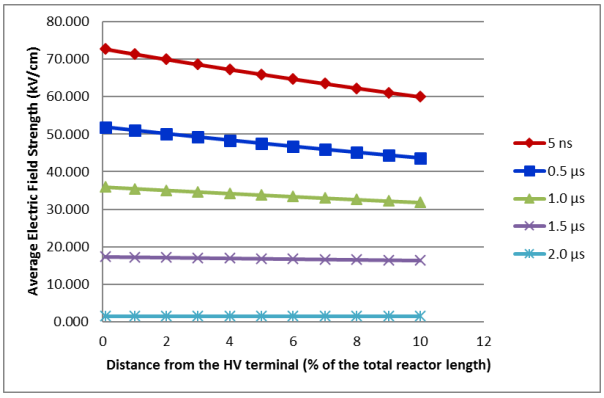

FIGURE 9. Average electric field strength along top 10% of reactor winding at different times following MSCDN energisation.

B. DIELECTRIC CURRENT IN THE INTER-TURN INSULATION

Winding insulation can incur damage from current flowing during transient events [6], [19], [20]. The resistive (leakage) current due to non-zero conductivity of the insulation material is usually small. However, the capacitive or displacement current representing the fast response associated with a change in the electric field amplitude can be significant. At the winding inter-turn insulation, this current can be expressed as:

$$i_{ct} = C_{tt}\left(\frac{dV_{tt}}{dt}\right) \tag{17}$$

Where i_{ct} is the capacitive current through insulation, C_{tt} the turn-to-turn capacitance, V_{tt} the turn-to-turn voltage and dt the voltage transition time

Since the capacitive current is voltage-dependent, an abrupt change in the voltage may produce a short burst of capacitive current. In this present work, the effect of the capacitive part of the dielectric current is examined during the worst MSCDN energisation condition. Under such condition, the capacitive current flowing during the 5ns voltage transition time associated with the worst-case MSCDN energization is calculated. Using Equations (13) and (15), the capacitive current flowing through the turn-to-turn winding insulation for the 400-kV reactor under study was approximately 347A, which is close to that shown in Fig. 8(b), where a high dV/dt results in a current surge of nearly 350 A flowing through the winding insulation and remains for the duration of the surge. In addition, the combined effect of this current added to the steady-state current that flows during normal operation could lead to excessive dielectric heating in the winding insulation. Furthermore, the occurrence of these currents is possible at every MSCDN energisation, which is performed several times per day. Over time, degradation in the insulation due to the cumulative effect of high dielectric current and applied electric field may be evident.

VI. EFFECT OF REACTOR PARAMETERS ON INTER-TURN FIELD AND CURRENT

A parametric analysis was conducted on the severely stressed areas by varying the reactor parameters within their specified limits, and the resulting field distribution is compared with the base case field distribution.

A. EFFECT OF DIELECTRIC RESISTANCE

The reactor voltage is more sensitive to the dielectric insulation resistance than to the winding resistance. The latter is true because of the large Q factor of the reactors, which results in time constants for the series branches that are much larger than the time periods considered in the transient analysis. To explore the effect of inter-turn insulation resistance on the electric field, the electric field strength across the upper 10% of the reactor was computed for low and high shunt resistances, and the results are shown in Fig. 10. As expected, a high value of dielectric resistance would reduce losses and allow high electric field magnitude to appear across the inter-turn insulation. If this resistance is lowered, significant losses occur and lower fields would result. It was found that the maximum voltage decreased by approximately 40% of the base case voltage for a reduction of 10 order-of-magnitudes in the shunt resistance. As a result, the maximum electric field strength applied on the winding insulation also decreased. The insulation resistance representing the losses between winding turns is dictated by several design factors such as type of dielectric material, insulation thickness, and the reactor diameter. In real applications, the use of high-resistivity dielectric materials for wrapping the winding conductors and

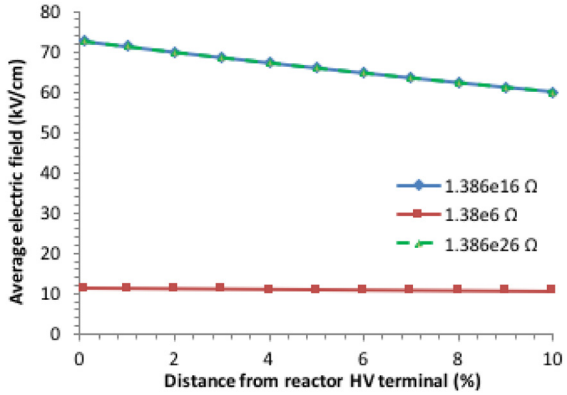

FIGURE 10. Effect of inter-turn insulation resistance on electric field.

insulation grading are important design solutions to help increase the insulation resistance.

B. EFFECT OF WINDING TURN INDUCTANCE

Fig. 11 shows the effect of winding inductance on the maximum electric field strength. These results were obtained by increasing, respectively decreasing, the inductance of each winding section by 50% of its base case value. As can be seen, the winding inductance has no effect on the electric field distribution. This is expected because the magnetic field in the inductance requires a build-up time higher than that over which the transient analysis is performed. Usually, when the applied voltage is maintained for a sufficient time, appreciable currents begin to flow in the inductances, leading to nearly uniform voltage distribution.

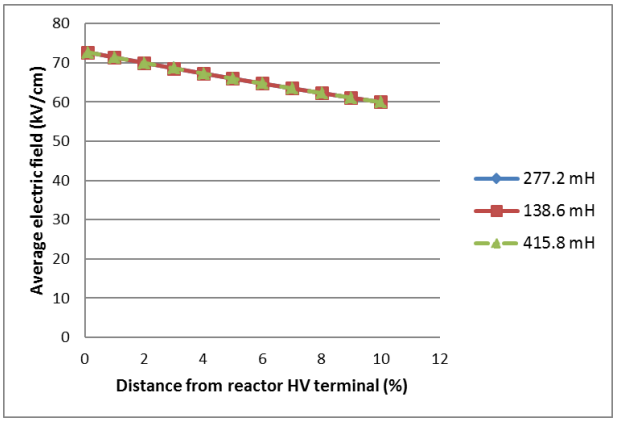

FIGURE 11. Effect of winding turn inductance on electric field.

C. EFFECT OF INTER-TURN CAPACITANCE

The effect of inter-turn capacitance on the electric field strength was considered for lower and higher inter-turn capacitances, relative to its base case value. Fig. 12 shows the electric field across the upper 10% of the reactor winding considered for three values of inter-turn capacitances: the base value which was computed using (13) as 19.16 pF, and the two other capacitances are one order of magnitude lower and one order of magnitude higher than the base value.

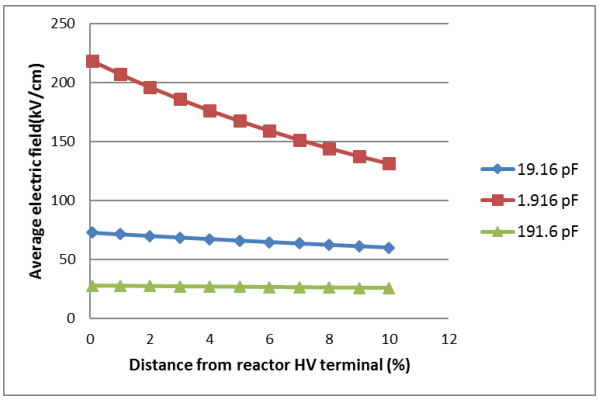

FIGURE 12. Effect of inter-turn capacitance on electric field.

For one order of magnitude decrease in the inter-turn capacitance, the voltage across the uppermost inter-turn winding was found to increase by approximately 200% from its base case value. The resultant electric field strength reached a maximum of about 220 kV/cm, which exceeds the manufacturer-specified dielectric strength for Mylar polyester film of 170 kV/cm [21]. Furthermore, it was found that low inter-turn capacitance may reduce the capacitive current that is flowing through the inter-turn winding insulation. Using Equation (17), the capacitive current obtained in this case was approximately 260 A, which is lower than the value of 350 A corresponding to the base case. On the other hand, the voltage distribution over the upper 10% of the reactor is greatly improved, and decreases by approximately 60% when the capacitance increases by one order of magnitude. Interleaving is used for increasing the inter-turn capacitance and improving the transient response of the windings, as is often used with transformers [22].

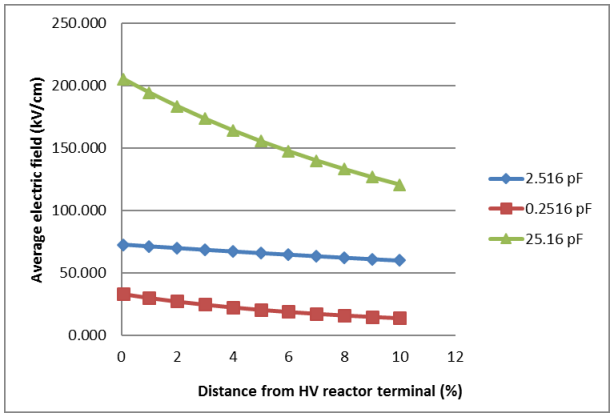

FIGURE 13. Effect of capacitance to ground on electric field.

D. EFFECT OF CAPACITANCE-TO-GROUND

Fig. 13 shows the electric field strength distribution on the upper 10% of the reactor winding considered for low and high capacitances-to-ground, obtained by decreasing, respectively increasing the base capacitance to ground of 2.516 pF calculated using (14) by one order of magnitude.

For high capacitance-to-ground, the maximum electric field strength increases by approximately 180% from the base-case value. Furthermore, increasing capacitance-to-ground may also increase the capacitive dielectric current flow of the inter-turn insulation. In this case, the capacitive current was approximately 380 A. For large reactor ratings, the capacitance-to-ground tends to become smaller relative to the inter-turn capacitance. Hence if the ground capacitance is reduced, more current will flow through the inter-turn capacitances, leading to more uniform voltage distribution along the winding.

In summary, a reduction of the electric field strength is obtained by increasing the inter-turn capacitance and reducing the capacitance-to-ground of the reactor. However, such a requirement of high inter-turn capacitance and low capacitance-to-ground is commonly associated with the reactor cost and design, as well as other electrical and mechanical factors. For instance, changing the insulation thickness and/or permittivity to increase the inter-turn capacitance may not be practically feasible as it may affect safety issues of the reactor design. A better alternative for controlling the capacitance-to-ground (Cg) is by changing the reactor height above ground. The capacitance-to-ground is also dependent on electrodes configuration, the radial gap and the circumferential areas between the windings. These parameters are usually fixed according to optimum electrical design considerations.

VII. POSSIBLE FAILURE MECHANISMS OF MSCDN REACTORS

From the previous analysis, the parameters having the most influence on transients and insulation failures occurring in the reactor windings are:

A. HIGH ELECTRIC FIELD STRENGTH

The model showed that during MSCDN energization, the reactor may be exposed to steep, high-magnitude overvoltages, which result in large potential differences across the inter-turn windings at the reactor HV terminal. This imposes high electric field on the insulation. The model computations revealed that a field strength of 72 kV/cm was obtained on the winding turns located at approximately 0.1% from the reactor HV terminal. Although this value is higher than its steady-state value, it is still below the dielectric strength of Mylar film specified by the manufacturer, which is 170 kV/cm. It is postulated that the electric field alone may not be the dominating factor that causes insulation failures in the reactor winding, but a repeated switching overvoltage at this level may contribute to degradation of the insulation.

B. HIGH RATE OF CHANGE OF VOLTAGE (dV/dt)

It was shown that energisation of the MSCDN results in an extremely high capacitive current on the inter-turn insulation of the reactor winding, which is directly proportional to the voltage rate of rise. The computed displacement current in the inter-turn insulation of approximately 350 A is by itself not harmful to the insulation until it reaches a sufficiently high level, and leads to some energy losses. A synergetic effect of dielectric stress and dielectric heating is believed to be the influencing failure mechanism of the reactor insulation failure. These are recurring phenomena and, combined with the continuous steady state currents and voltages, may lead to failure over a long period.

C. EFFECT OF SURGE ARRESTER OPERATION

In Fig. 4, surge arresters were installed across the filter reactor and the damping resistor, respectively to provide necessary protection against overvoltages. Figure 14(a) shows the voltage across the filter reactor when the MSCDN was switched in at the instant of voltage maximum. The current through the surge arrester connected parallel to the filter reactor is shown in Fig. 14(b).

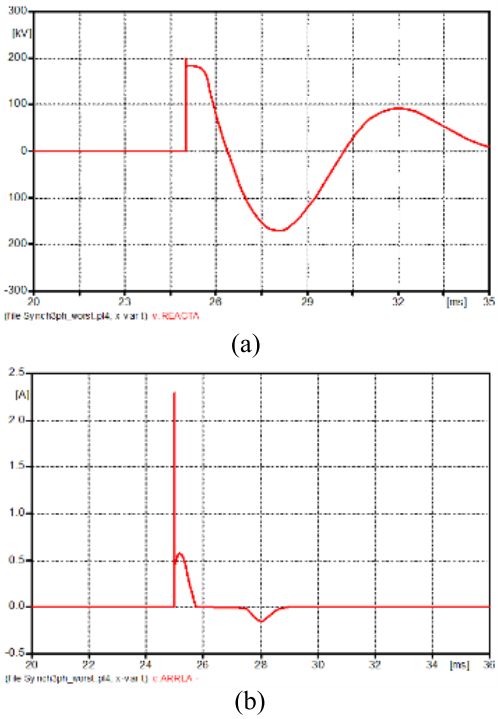

FIGURE 14. (a) Reactor voltage and (b) Surge arrester current following MSCDN energization

As can be seen, even though the magnitude of the arrester current is small, its rate-of-rise is very high. The surge arrester operated at voltage maximum around t = 25 ms. Near to the voltage peak, a rapid voltage spike is observed. This spike was not observed when the reactor was energized without the surge arrester. Hence, surge arrester operation may cause additional stress on the reactor insulation when energised at unfavourable time instants.

VIII. CONCLUSION

A model of a vertically-mounted single-layer air-core reactor of a 400-kV MSCDN is developed using a lumped parameter approach. The model was implemented in ATP/EMTP and the results showed that the transient voltage and field distributions along the reactor winding are highly non-uniform at

instants immediately following switching, with the highest values occurring in the upper 10% of the reactor winding. A parametric analysis showed the effects of reactor parameters on the field strength stressing the reactor insulation, and possible failure mechanisms were identified. Practical methods for mitigating stress during MSCDN switching such as insulation grading and improved design are described.

REFERENCES

[1] R. C. Campos, D. O. Lacerda, and M. F. Alves, "Mechanically switched capacitor with damping network (MSCDN)-engineering aspects of application, design, and protection," in *Proc. IEEE/PES Transmission Distrib. Conf. Expo., Latin Amer.*, Nov. 2010, pp. 316–322.

[2] *IEEE Standard Requirements, Terminology, and Test Code for Dry-Type Air-Core Series-Connected Reactors*, IEEE Standard C57.16-1996, 2011.

[3] A. M. Mahdy, A. El-Morshedy, and H. I. Anis, "Insulation failure assessment under random energization overvoltages," *IEEE Trans. Ind. Appl.*, vol. 32, no. 2, pp. 214–220, Mar. 1996.

[4] X. Wei, C. Shukang, and W. Jianér, and W. Yonghong, "Research on turn-to-turn insulation test method of dry-type air-core reactor," in *Proc. 6th Int. Conf. Properties Appl. Dielectr. Mater.*, vol. 2, 2000, pp. 1058–1061.

[5] Y. Xiuke and Y. Jian, "Calculation of wave process in an air core reactor," in *Proc. Int. Conf. Energy Environ. Technol. (ICEET)*, 2009, pp. 96–98.

[6] *Evaluation and Qualification of Electrical Insulation Systems*, Standard BS EN 60505, 2011.

[7] M. M. A. Salama, "A calcualtion method for voltage distribution in a large AIR core power reactor," *IEEE Trans. Power App. Syst.*, vol. PAS-100, no. 4, pp. 1752–1758, Apr. 1981.

[8] S. L. Varricchio and N. H. C. Santiago, "Transient voltage distribution in air core reactors," in *Proc. 8th Int. Symp. High Voltage Eng. (ISH)*, Yokohama, Japan, 1993, pp. 221–224.

[9] S. L. Varricchio and N. H. C. Santiago, "Electrical strength in air core reactors," in *Proc. 4th Int. Conf. Properties Appl. Dielectr. Mater.*, Brisbane, QLD, Australia, 1994, pp. 221–224.

[10] M. Popov, L. V. D. Sluis, R. P. P. Smeets, J. Lopez-Roldan, and V. V. Terzija, "Modelling, simulation and measurement of fast transients in transformer windings with consideration of frequency-dependent losses," *IET Electr. Power Appl.*, vol. 1, no. 1, pp. 29–35, Jan. 2007.

[11] M. Popov, R. P. P. Smeets, L. Van der Sluis, H. De Herdt, and J. Declercq, "Analysis of voltage distribution in transformer windings during circuit breaker prestrike," in *Proc. Int. Conf. Power Syst. Transients (IPST)*, Kyoto, Japan, Jun. 2009, pp. 1–6.

[12] M. M. A. Salama, R. F. Dudley, and G. Gela, "Calculation of steady-state surface at winding ends of air-core power reactors," *IEEE Trans. Power App. Syst.*, vol. PAS-100, no. 7, pp. 3673–3678, Jul. 1981.

[13] A. A. Dahab, P. E. Burke, and T. H. Fawzi, "A complete model of a single layer air-cored reactor for impulse voltage distribution," *IEEE Trans. Power Delivery*, vol. PWRD-3, no. 4, pp. 1745–1753, Oct. 1988.

[14] P. Holmberg, "Modelling the transient response of windings, laminated steel coresand electromagnetic power devices by means of lumped circuits," Ph.D. dissertation, Dept. High Voltage Res., Uppsala Univ., Uppsala, Sweden, 2000.

[15] M. Enohnyaket, "PEEC modelling and verification for broadband analysis of air-core reactors," Ph.D. dissertation, Dept. Comput. Sci. Elect. Eng., Lulea Univ. Technol., Lulea, Sweden, 2007.

[16] A. Greenwood, *Electrical Transients in Power Systems*, 2nd ed. New York, NY, USA: Wiley, 1991.

[17] F. Grover, *Inductance Calculations; Working Formulas and Tables*. New York, NY, USA: Van Nostrand, 1946.

[18] P. S. Maruvada and N. Hylten-Cavallius, "Capacitance calculations for some basic high voltage electrode configurations," *IEEE Trans. Power App. Syst.*, vol. PAS-94, no. 5, pp. 1708–1713, Sep. 1975.

[19] C. Mayoux, "Degradation of insulating materials under electrical stress," *IEEE Trans. Dielectr. Electr. Insul.*, vol. 7, no. 5, pp. 590–601, Oct. 2000.

[20] R. Bruetsch, M. Tari, K. Froehlich, T. Weiers, and R. Vogelsang, "High voltage insulation failure mechanisms," in *Proc. IEEE Int. Symp. Elect. Insul. (ISEI)*, Jun. 2008, pp. 162–165.

[21] Goodfellow, United Kingdom. (2018). *Product Information*. [Online]. Available: http://www.goodfellow.com/E/Polyethylene-terephthalate.html

[22] M. J. Heathcote, *The J&P Transformer Book*, 12th ed. Great Britain, U.K.: Newnes, 1998.

HAZIAH ABDUL HAMID (M'13) received the Bachelor and master's degrees in electrical engineering from Universiti Teknologi Malaysia in 1999 and 2002, respectively, and the Ph.D. degree in electrical and electronic engineering from Cardiff University, U.K., in 2012. She is currently a Senior Lecturer and the Dean with the School of Electrical System Engineering, Universiti Malaysia Perlis, Malaysia. Her main research interests are in high voltage transients, insulation system, and earthing system.

NOUREDDINE HARID (M'13) received the Ph.D. degree in electrical engineering from Cardiff University, U.K., in 1992. Since 1992, he has been with Academia as an Assistant Professor and an Associate Professor. He joined Cardiff University in 2001. Since 2017, he has been an Associate Professor with the Khalifa University of Science and Technology, Abu Dhabi. His main research interests are in earthing systems, insulation systems, transients, breakdown phenomena, and condition monitoring of high-voltage equipment. He is a member of IET and a fellow of the Higher Education Academy and served as a member of the BSI GEL/81 Standard Committee on Lightning Protection.

MANU A. HADDAD (M'13) received the Bachelor degree in electrical engineering in 1985 and the Ph.D. degree in high voltage engineering in 1990. He is currently a Professor in electrical engineering with Cardiff University, with responsibility for research in high voltage engineering. His research interests are in overvoltage protection, insulation systems, insulation coordination, and earthing of electrical energy systems. He has published an IET-Power Series Book on *Advances in High Voltage Engineering*. He is a member of the CIGRE Working Groups and a member of BSI PEL1/2, IEC TC37. He serves on the scientific committees of several international conferences.

HUW GRIFFITHS (M'14) received the B.Sc. degree in electrical and electronic engineering from the Polytechnic of Wales and the Ph.D. degree in electrical engineering from Cardiff University, Cardiff, U.K. From 1983 to 1990, he was an Engineer in distribution and transmission system design for SWaEB and CEGB, respectively. In 1990, he joined Cardiff University as a Lecturer, and researching with the high voltage group, he became a Senior Lecturer, a Reader, and a Professor. In 2015, he moved as a Professor to the Khalifa University of Science and Technology, Abu Dhabi. His research interests are grounding systems, transients, and high voltage insulation. Over many years, he has been a member of several British Standards, CENELEC, IEC, CIGRE, and CIRED committees, and working groups related to grounding systems. He is a Chartered Engineer, and a member of IET.